Optimal Energy Management and Sizing of a Dual Motor-Driven Electric Powertrain

Xiaosong Hu, *Senior Member, IEEE*, Yapeng Li, Chen Lv, *Member, IEEE*, and Yonggang Liu, *Member, IEEE*

***Abstract*—This paper is concerned with combined power-source sizing and energy management optimization for multi-motor-driven electric powertrains. Existing studies focus mostly on adopting heuristically determined battery and motor sizes for such powertrains, without a sufficient exploration of the coupling between power-source dimension and energy management strategy. To address this research gap, this paper aims at presenting an alternative, convex programming based method to optimize the multi-power-source integration problem, for vehicular economy maximization. Specifically, for the first time, we leverage this method to optimize an electric bus powertrain configuration with front-and-rear-axle dual motors and a clutch, as a case study. Numerous analysis results, as well as comparisons with common design/control practice, demonstrate the effectiveness and computational benefit of the proposed scheme.**

***Index Terms*—Batteries, component sizing, electric drive, electric vehicle (EV), energy management, optimization.**

I. Introduction

A. Motivation and Technical Challenge

INCREASINGLY stringent standards and regulations on emissions of carbon dioxide and harmful tail-pipe pollutants constitute an overwhelming driving force for the development and deployment of electric vehicles (EV) over the world [1]. Despite a promising interplay with renewables for a sustainable energy future, EVs are still facing with some technological and cost shortcomings, mainly owing to the state of the art of commercial traction batteries [2]. The material and chemical aspects have a decisive impact on the overall battery performance [3]. Up to date, no adequate breakthroughs make energy

Manuscript received July 6, 2018; revised September 10, 2018; accepted October 22, 2018. Date of publication October 31, 2018; date of current version May 22, 2019. This work was supported in part by the EU-funded Marie Sklodowska-Curie Individual Fellowships (IF) Project under Grant 706253-pPHEV-H2020-MSCA-IF-2015 and in part by the Fundamental Research Funds for the Central Universities of China under Grants 106112016CDJXZ338825, 106112017CDJQJ338811, and 2018CDQYQC0035. Recommended for publication by Associate Editor M. Ferdowsi. *(Corresponding authors: Xiaosong Hu and Chen Lv.)*

X. Hu is with the State Key Laboratory of Mechanical Transmissions, Department of Automotive Engineering, Chongqing University, Chongqing 400044, China, and with Advanced Vehicle Engineering Centre, Cranfield University, Cranfield MK43 0AL, U.K. (e-mail:

common is four-wheel independent actuation via four in-wheel motors [26]–[32]. The configuration of four onboard motors and four individual gearboxes was also introduced in [33] to realize four-wheel independent control. The work in [34] unveiled a combination of four motors with a transmission to drive the rear axle.

2) Energy Management: How to control multiple motors in harmony is an enabling technology in advanced electric powertrains. Specifically, energy management herein means power split or torque distribution among multiple motors. Depending on the overall control objective, energy management techniques can be roughly divided into the following two categories.

The first category is concerned with vehicular active safety and/or maneuverability, with a particular consideration of tire-road interactions. For example, a sliding mode control was developed in [9] to regulate the slip ratio on each wheel within a desirable region for an EV with front-and-rear-axle dual motors. Since this type of energy management is not the focus of our work, interested readers are referred to a comprehensive review article [33] for more relevant information.

The second category is targeted at improving energy efficiency of electric powertrains, where vehicular maneuver control is sometimes also integrated. For instance, a rule-based algorithm was applied in [15] to realize a two-mode energy management strategy for a dual-motor EV with a planetary gear set. In order to further increase energy efficiency of such dual-motor powertrains, some optimization-based energy management strategies were also synthesized, e.g., dynamic programming (DP) [17] and model predictive control [20]. As for powertrains with front-and-rear-axle dual motors, analytical solutions of optimal energy management were explored by deriving analytical power losses of motors [10, 11]. When using two identical motors, even torque distribution is found to be the optimal control. Moreover, the results in [11] demonstrate that a clutch is advantageous to further reducing energy consumption through turning OFF one motor, when the torque demand is lower than a threshold. The study in [13] discusses maximizing the powertrain efficiency when the two motors have different sizes, where a fuzzy-logic clutch controller is exploited to govern the transition between single-motor and dual-motor modes. Additionally, four different optimization algorithms are contrasted in [12] for minimizing energy consumption of a front-and-rear-axle-driven electric wheel loader. As for four-motor powertrains, optimal analytical energy management was examined as well. The optimality of even torque distribution among four motors, given assumptions that four electric drivetrains are the same, and that the drivetrain power loss is strictly monotonically increasing versus the wheel torque, is shown in [27]. Moreover, [28] presents an analytical solution taking loading transfer into account. In the case of four motors of different sizes, the analytical energy management has been investigated in [29]. An iterative search of optimal torque distribution among four motors was devised in [30]. In addition, with topography preview, DP was leveraged in [26] to accomplish both the optimal vehicle speed and optimal torque distribution among four in-wheel motors. A multi-objective optimization approach was also put forward to evaluate tradeoffs between energy consumption and vehicular maneuverability in a hierarchical manner [31].

3) Component Sizing: Component sizing plays an important role in performance and fuel economy of electric powertrains as well. Particularly, sizes of the battery system and motors should be meticulously designed. Nonetheless, compared to energy management research, fewer studies have been carried out on component sizing of multi-motor electric powertrains. The motor size and transmission gear ratios of a dual-motor EV were determined in [8] to meet vehicular power requirements, i.e., top vehicle speed, acceleration time, and maximum grade. With the goal of minimizing energy consumption, a cascaded bi-level component sizing scheme has been often used, where sizing optimization is conducted in the outer level, and energy management of multiple motors in the inner level. For example, the motor size and gear ratios of a dual-motor EV in [18] with a planetary gear set were optimized by multi-objective particle swarm optimization (PSO) algorithm in the outer level, and the inner-level energy management strategy was rule based. Similarly, the motor sizes, battery capacity, and planetary gear set parameters were optimized in [19] by using quantum genetic algorithm. However, rule-based energy management in the inner level invariably leads to non-optimal torque distribution. To address this deficiency, for a rear-axle-driven EV with dual motors in [22], a convex optimization-based energy management strategy was harnessed in the inner level to ensure optimality and computational rapidness of power split, while genetic search algorithm was employed in the outer level to optimize sizes of the battery pack and motors. For the four-motor rear-axle-driven EV in [34], a divide-and-conquer approach was utilized for optimal torque distribution, and genetic algorithm for transmission gear ratio optimization. The four-in-wheel-motor-driven EV in [32] adopted an adaptive torque distribution method and PSO in the outer level to optimize sizes of four motors and the battery pack.

C. Research Gap and Original Contributions

The vast majority of existing efforts focused on energy management optimization of multi-motor electric powertrains, given identical parameters of motors or electric drivetrains. A few of studies attempted to synergize energy management with component sizing for these powertrains via a bi-level optimization scheme. However, the often-used evolutionary algorithms in the outer level are invariably computationally inefficient and inherently cannot guarantee a globally optimal sizing outcome. For example, in [22], the sizing optimization still took more than 12 h, even though a rapid, convex programming-based energy management algorithm was applied. Therefore, a computationally efficient, joint optimization framework of component sizing and energy management is still lacked such that energy-saving benefits of multi-motor electric powertrains cannot be fully explored.

Strongly motivated by this research gap, we extend convex programming, a recognized efficient tool for combined design and control optimization of hybrid vehicles [35]–[38], to multi-motor electric powertrains. This article presents, for the first time, a quick, simultaneous optimization of energy management and motor/battery dimension for the powertrain configuration with front-and-rear-axle dual motors and a clutch, as a case study. As a result, the following interesting questions

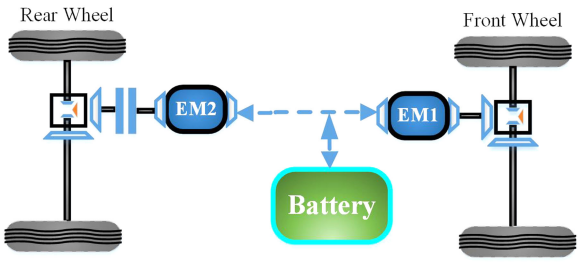

Fig. 1. Configuration of the electric bus powertrain system.

about this configuration that remained unanswered before can be addressed:

1) Can two motors of different sizes make the powertrain more energy-efficient than a common paradigm of using two identical motors?
2) Is it possible to establish a systematic method to determine sizes of the two motors? Is such a method useful to guide the dual-motor integration, e.g., into Tesla P100D?
3) How does the motor/battery sizing interact with the torque distribution between dual motors to maximize the powertrain efficiency?

D. Paper Organization

The rest of the paper is structured as follows. The powertrain model is introduced in Section II. Section III formulates the convex programming framework for combined component sizing and energy management. Results and discussion are presented in Section IV, followed by key conclusions drawn in Section V.

II. Powertrain Modeling

As shown in Fig. 1, the considered dual-motor arrangement for an electric bus consists of EM1 and EM2 mounted at the front and rear axles, respectively. Furthermore, a clutch is placed between EM2 and the rear axle, in order to isolate (turn OFF) EM1 when the road load is low.

A. Power Balance

In the course of vehicle traveling, the powertrain must fulfill road power/torque demand. The battery powers the two motors (EM1 and EM2), through which electric energy is converted into mechanical energy to drive the vehicle. During braking, both motors can recuperate the mechanical energy through the braking torque and store the recuperated energy into the battery. When the braking torque is larger than the recuperation limit, a friction braking serves as a supplement. If the vehicle velocity and road slope are known *a priori*, the traction force F_t at the wheels at time k can be calculated according to longitudinal vehicular dynamics:

$$F_t(k) = \frac{c_d A_f \rho v(k)^2}{2} + m_{\text{tot}} g c_r \cos(\beta(k)) + m_{\text{tot}} g \sin(\beta(k)) + m_{\text{tot}} a(k) \quad (1)$$

$$m_{\text{tot}} = m_{\text{veh}} + m_{\text{EM1}} + m_{\text{EM2}} + m_{\text{bat}} \quad (2)$$

TABLE I
Main Vehicular Parameters [35]

Name	value	unit
Chassis mass m_{veh}	13700	kg
Front area A_f	7.54	m^2
Rolling resistance c_r	0.007	/
Aerodynamic drag c_d	0.7	/
Wheel radius r_w	0.509	m
Final gear i_0	4.7	/
Chassis inertia J_{chs}	41.8	kgm^2
Auxiliary power P_{aux}	7	kW
Air density ρ	1.1839	kg/m^3
Gravity g	9.8100	m/s^2

where c_d is the aerodynamic drag coefficient, A_f is the vehicular front area, ρ is the air density, v is the vehicular longitudinal velocity, m_{tot} is the total mass of vehicle, g is the gravity acceleration, c_r is the rolling resistance coefficient, β is the road slope, and a is the acceleration. Moreover, m_{veh} is the chassis mass, m_{EM1} is the front motor mass, m_{EM2} is the rear motor mass, and m_{bat} is the battery mass. Based on (1) and (2), the power demand P_{dem} and torque demand T_{dem} at the EM1/EM2 shaft can be calculated as

$$J_{\text{veh}} = J_{\text{chs}} + (J_{\text{EM1}} + J_{\text{EM2}}) i_0^2 \quad (3)$$

$$T_{\text{dem}}(k) = \frac{F_t(k) r_w}{i_0} + \frac{J_{\text{veh}} a(k)}{r_w i_0} \quad (4)$$

$$P_{\text{dem}}(k) = F_t(k) v(k) + \frac{J_{\text{veh}} a(k) v(k)}{r_w^2} \quad (5)$$

where r_w is the effective wheel radius, i_0 is the final drive gear, J_{veh} is the total inertia of vehicle chassis including wheels, J_{EM1} and J_{EM2} are the inertias of both motors. The key vehicle specifications are listed in Table I.

The power balance at time k can then be written as

$$\sum_{i=1}^{2} P_{\text{EM}i,\text{input}}(k) - \sum_{i=1}^{2} P_{\text{EM}i,\text{loss}}(k) = P_{\text{dem}}(k) \quad (6)$$

where $P_{\text{EM}i,\text{input}}$ is the input power of motor, and $P_{\text{EM}i,\text{loss}}$ is the power loss of motor (including inverter losses). Therefore, the battery output power is described by

$$P_{\text{bat}}(k) = \sum_{i=1}^{2} P_{\text{EM}i,\text{input}}(k) + P_{\text{aux}}(k) \quad (7)$$

where P_{bat} is the battery output power, and P_{aux} is the auxiliary power of vehicle.

B. Motor Model

The power loss of motor is an important consideration in developing EV energy management strategies. It is of particular importance to ensure a high-efficiency motor operation. In this paper, the motor power loss is approximated by a quadratic

TABLE II
BASELINE MOTOR PARAMETERS

Name	EM1	EM2	unit
Peak power	70	100	kW
Inertia	0.7319	1.0454	kgm2
Mass	95.46	136.35	kg
Max torque	1622.8	2318.0	Nm

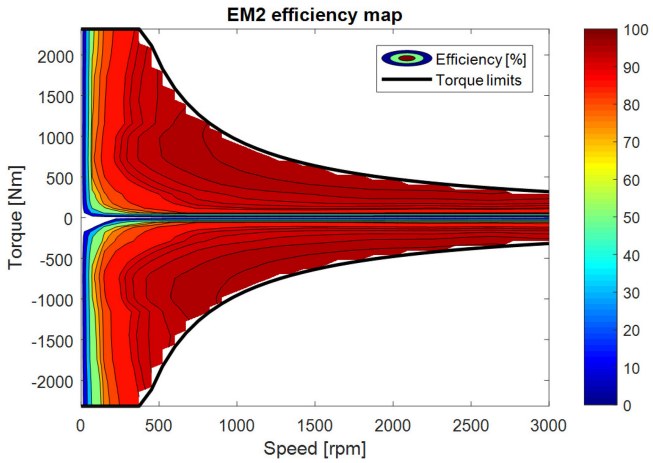

Fig. 2. Baseline EM2 efficiency map [40].

function as follows [35]–[39]:

$$P_{\mathrm{EM}i,\mathrm{loss}}(k) = a_{i1}(k)T_{\mathrm{EM}i}(k)^2 + a_{i2}(k)T_{\mathrm{EM}i}(k) + a_{i3}(k) \tag{8}$$

and the motor input power is written by

$$P_{\mathrm{EM}i,\mathrm{input}}(k) = P_{\mathrm{EM}i,\mathrm{loss}}(k) + T_{\mathrm{EM}i}(k)\omega_{\mathrm{EM}i}(k) i = 1,2 \tag{9}$$

where a_{i1}, a_{i2}, and a_{i3} are functions of the motor rotational speed $\omega_{\mathrm{EM}i}$.

The main parameters of the baseline EM1 and EM2 are listed in Table II. The efficiency map of the baseline EM2 is shown in Fig. 2 [40].

To size EM1/EM2, the EM maximum and minimum output torques are scaled by s_{EM} [41], and the EM power loss is assumed to change with a baseline value linearly [37], [42]:

$$T_{\mathrm{EM}}(k) \in [T_{\mathrm{EMmin,base}}, T_{\mathrm{EMmax,base}}]s_{\mathrm{EM}} \tag{10}$$

$$P_{\mathrm{EM,loss}} = s_{\mathrm{EM}} P_{\mathrm{EM,loss,base}} \tag{11}$$

where $T_{\mathrm{EMmin,base}}$ and $T_{\mathrm{EMmax,base}}$ are baseline torque limits.

Consequently, the power loss of motor

$$\begin{aligned} P_{\mathrm{EM,loss}}(k) &= s_{\mathrm{EM}} P_{\mathrm{EM,loss,base}}(k) \\ &= s_{\mathrm{EM}}(a_1(k)T_{\mathrm{EM,base}}(k)^2 \\ &\quad + a_2(k)T_{\mathrm{EM,base}}(k) + a_3(k)) \\ &= s_{\mathrm{EM}}\left(a_1(k)\left(\frac{T_{\mathrm{EM}}(k)}{s_{\mathrm{EM}}}\right)^2\right. \\ &\quad \left. + a_2(k)\frac{T_{\mathrm{EM}}(k)}{s_{\mathrm{EM}}} + a_3(k)\right) \\ &= a_1(k)\frac{T_{\mathrm{EM}}(k)^2}{s_{\mathrm{EM}}} + a_2(k)T_{\mathrm{EM}}(k) + a_3(k)s_{\mathrm{EM}} \end{aligned} \tag{12}$$

and then the EM1/EM2 power loss and input power can be calculated by

$$\begin{aligned} P_{\mathrm{EM}i,\mathrm{loss}}(k) &= a_{i1}(k)\frac{T_{\mathrm{EM}i}(k)^2}{s_{\mathrm{EM}i}} \\ &\quad + a_{i2}(k)T_{\mathrm{EM}i}(k) + a_{i3}(k)s_{\mathrm{EM}i} i = 1,2 \end{aligned} \tag{13}$$

$$P_{\mathrm{EM}i,\mathrm{input}}(k) = P_{\mathrm{EM}i,\mathrm{loss}}(k) + T_{\mathrm{EM}i}(k)\omega_{\mathrm{EM}i}(k) \tag{14}$$

where $s_{\mathrm{EM}i}$ is the motor scaling factor. The maximal output power of motor is calculated by

$$P_{\mathrm{EM}i\max} = P_{\mathrm{EM}i\max,\mathrm{base}} s_{\mathrm{EM}i} \tag{15}$$

where $P_{\mathrm{EM}i\max,\mathrm{base}}$ is the maximal output power of baseline motor.

Normally, the mass and inertia of a motor are related to its rotor diameter. In order to simplify the algorithm and increase the powertrain simulation efficiency, the mass and inertia of each motor have been assumed to change linearly with a baseline value [37], which have been used and justified in [43], [44]. The motor inertia and mass are scaled by

$$J_{\mathrm{EM}i} = J_{\mathrm{EM}i,\mathrm{base}} s_{\mathrm{EM}i} i = 1,2 \tag{16}$$

$$m_{\mathrm{EM}i} = m_{\mathrm{EM}i,\mathrm{base}} s_{\mathrm{EM}i} i = 1,2 \tag{17}$$

where $J_{\mathrm{EM}i,\mathrm{base}}$ and $m_{\mathrm{EM}i,\mathrm{base}}$ are the inertia and mass of baseline motor, respectively.

C. Battery Model

The opened circuit voltage (OCV) of lithium-ion battery is closely related to its state of charge (SOC). It is illustrated in [39] that in a common SOC range for vehicular applications, the OCV almost exhibits a linear relationship with SOC. Therefore, here, for a battery cell, the relationship between the OCV (V_{oc}), and SOC is written as

$$V_{\mathrm{oc}}(k) = \frac{Q}{C}\mathrm{SOC}(k) + V_0 \tag{18}$$

where Q is the cell capacity, C is a coefficient in [F] , and V_0 is the OCV value when SOC is equal to zero. The battery cell power includes two parts:

$$P_{\mathrm{bat,total}}(k) = P_{\mathrm{bat}}(k) + P_{\mathrm{bat,loss}}(k) \tag{19}$$

TABLE III
BATTERY CELL SPECIFICATIONS

Name	value	unit
Cell mass[a]	0.07	kg
Cell resistance[a]	0.01	Ω
Maximum discharge current[a]	-35	A
Maximum charge current[a]	35	A
Cell capacity[a]	8280	As
$n_{\text{bat,base}}$	1800	/

[a]is from [46].

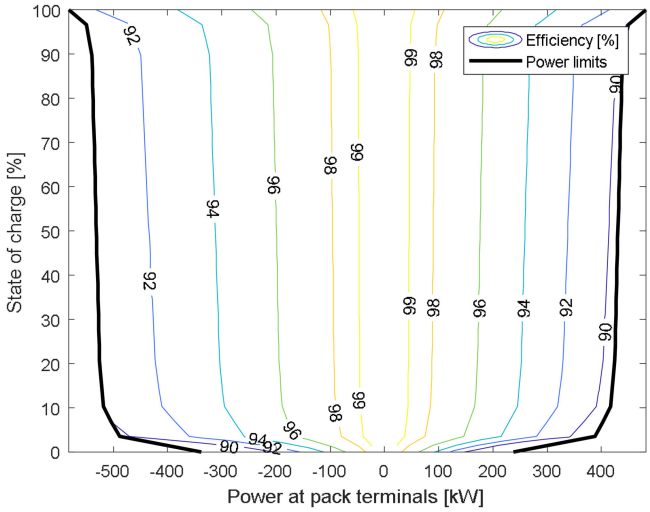

Fig. 3. Baseline battery pack efficiency map [46], [47].

where $P_{\text{bat,total}}$ is the battery cell internal power, and P_{bat} and $P_{\text{bat,loss}}$ are the battery cell terminal power and power loss, respectively.

As the battery cell resistance is assumed to be a constant, the battery cell power loss can be calculated by

$$P_{\text{bat,loss}}(k) = I(k)^2 R \tag{20}$$

$$P_{\text{bat}}(k) = V_{\text{oc}}(k) I(k) - I(k)^2 R \tag{21}$$

where I is the battery cell current and R is the battery cell internal resistance. While the battery resistance varies with battery operating states (charging or discharging), such a change is relatively small, and during powertrain system-level controls and sizing, its impact on the optimization results of battery and EM sizes is often neglected. Hence, it is here reasonable to adopt a constant resistance during the optimization process, as treated in many relevant studies, e.g., [39].

In order to size the battery system, we introduce a scaling variable s_{bat}, $s_{\text{bat}} = n_{\text{bat}}/n_{\text{bat,base}}$, where n_{bat} is the number of cells in the target battery pack, and $n_{\text{bat,base}}$ is the number of cells in the baseline pack, which equals 1800. The main battery cell specifications are listed in Table III. And its efficiency map is shown in Fig. 3. Accordingly, the battery pack total power $\tilde{P}_{\text{bat,total}}$ to be optimized can be formulated as

$$\tilde{P}_{\text{bat,total}}(k) = V_{\text{oc}}(k) I(k) n_{\text{bat,base}} s_{\text{bat}}. \tag{22}$$

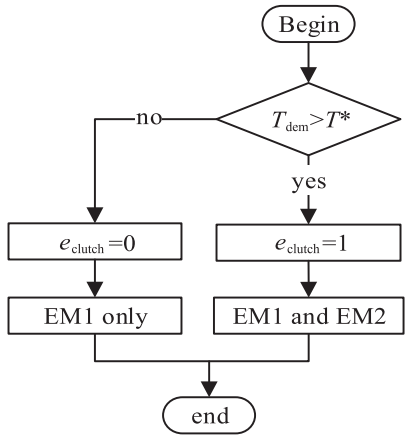

Fig. 4. Clutch control logic flowchart.

The battery state of energy is expressed by [36], [45]

$$\begin{aligned} E_{\text{bat}}(k) &= n_{\text{bat,base}} s_{\text{bat}} Q \int_0^{\text{SOC}(k)} V_{\text{oc}}(k) d\text{SOC}(k) \\ &= n_{\text{bat,base}} s_{\text{bat}} Q \int_0^{\text{SOC}(k)} \left(\frac{Q}{C} \text{SOC}(k) + V_0 \right) d\text{SOC}(k) \\ &= \frac{n_{\text{bat,base}} s_{\text{bat}} C}{2} (V_{\text{oc}}(k)^2 - {V_0}^2). \end{aligned} \tag{23}$$

The cell current limits are converted to the following power constraints:

$$\tilde{P}_{\text{bat,total}}(k) \geq V_{\text{oc}}(k) I_{\min} n_{\text{bat,base}} s_{\text{bat}} \tag{24}$$

$$\tilde{P}_{\text{bat,total}}(k) \leq V_{\text{oc}}(k) I_{\max} n_{\text{bat,base}} s_{\text{bat}} \tag{25}$$

where $I_{\min}$ and $I_{\max}$ are the allowable maximum charge current and discharge current, respectively.

The battery pack mass m_{bat} is scaled by

$$m_{\text{bat}} = m_{\text{bat,base}} s_{\text{bat}} \tag{26}$$

where $m_{\text{bat,base}}$ is the mass of the baseline battery pack.

D. Clutch Model

As mentioned before, power losses of both motors could account for a noticeable proportion in the total loss of the electric powertrain. As a result, an effective control of the clutch between EM2 and the drive shaft is useful to improve the EM2 efficiency by turning OFF the motor at low load [11], [48]–[50]. In this paper, we utilize a binary variable e_{clutch} to represent the clutch working state

$$e_{\text{clutch}} = \begin{cases} 1 & \text{clutch is engaged} \\ 0 & \text{clutch is disengaged.} \end{cases}$$

A heuristic control mechanism is used to determine e_{clutch}. Namely, when the vehicular torque demand T_{dem} is larger than a preset torque threshold, the clutch is engaged. To find an optimized torque threshold T^*, we run the inner-level convex programming over an outer-level grid of the torque threshold. The flowchart of the clutch control logic is shown in Fig. 4.

TABLE IV
PARAMETERS IN THE OBJECTIVE FUNCTION

Name	value	unit
P_{elt} [a]	0.196	euro/kWh
p_c [b]	5%	/
y_v [c]	5	year
s	70000	km
cost_{bat} [c]	6.831	euro
cost_{EM} [b]	20	euro/kW

[a]is from [54], [b] is from [53], [c] is from [39].

III. Optimization Problem Formulation

In this section, the convex optimization problem for the electric powertrain is mathematically formulated. First, we briefly introduce the definition of a generic convex programming problem. Then, how to construct the convex optimization of the specific powertrain is elaborated.

A. Definition of Convex Programming

A standard convex programming problem consists of an objective function and equality/inequality constraints with respect to optimization variables as follows [36], [45]:

$$\begin{aligned} &\text{minimize} \quad f(x) \\ &\text{subject to} \quad g_i(x) \leq 0,\ i = 1, ..., m \\ &\qquad\qquad Ax = b \end{aligned} \tag{27}$$

where $x = (x_1, ..., x_n)$ is the vector of optimization variables, $f(x)$ a convex objective function, $g_i(x)$ convex inequality constraints, and $Ax = b$ affine equality constraints. It is theoretically proven that a convex programming problem results in a unique global optimal solution, which can be rapidly solved by many commercial solvers, e.g., CVX [51], [52].

B. Objective Function

The objective function is to minimize the sum of electricity cost and depreciated battery/motor costs over a given driving cycle, as described by [40], [53]

$$\text{cost} = \text{cost}_{\text{op}} + \text{cost}_{\text{comp}} \tag{28}$$

where cost_{op} is the operational cost, i.e., electricity expenditure, defined as

$$\text{cost}_{\text{op}} = We(E_{\text{bat}}(1) - E_{\text{bat}}(\text{end})) \tag{29}$$

where We is the electricity consumption coefficient in [euro/Ws/100 km], which can be defined as

$$We = \frac{P_{\text{elt}}}{36d} \tag{30}$$

where P_{elt} is the electricity price in [euro/kWh], and d is the distance over drive cycle in [m]. In this way, the unit of the operational cost can be consistent with the component cost shown as follows:

$$\text{cost}_{\text{comp}} = W_b s_{\text{bat}} + \sum_{i=1}^{2} W_{\text{EM}} s_{\text{EM}i} \tag{31}$$

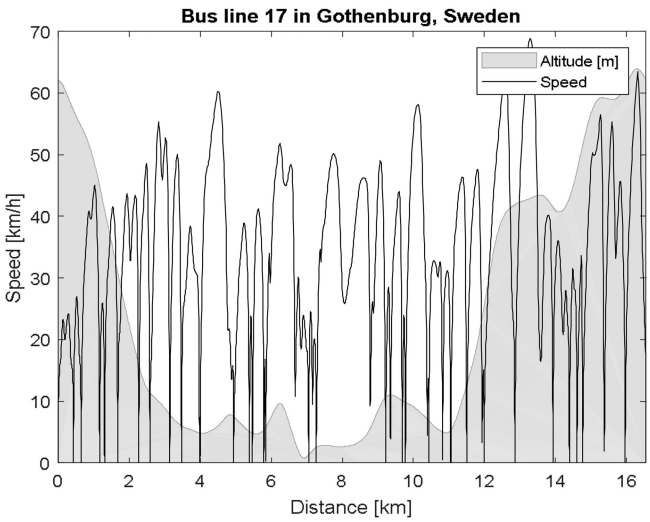

Fig. 5. Gothenburg, Sweden, driving cycle [35].

with W_b being the battery cost factor and W_{EM} the motor cost factor

$$W_b = 100000\ n_{\text{bat,base}} \text{cost}_{\text{bat}} \frac{1}{sy_v} \left(1 + p_c \frac{yv}{2}\right) \tag{32}$$

$$W_{\text{EM}} = 1000000\ P_{\text{EMimax,base}} \text{cost}_{\text{EM}} \frac{1}{sy_v} \left(1 + p_c \frac{y_v}{2}\right) \tag{33}$$

where cost_{bat} and cost_{EM} are the battery cell cost and EM cost per kW, s is the average yearly traveled distance, p_c is the yearly interest rate, and y_v is the vehicle service period. The values of the related parameters are listed in Table IV.

C. Optimization Formulation

According to (1), (2), (4), (17), and (26), the torque demand can be written as

$$T_{\text{dem}}(k) = T_0(k) + T_1(k) s_{\text{bat}} + T_2(k) s_{\text{EM1}} + T_3(k) s_{\text{EM2}} \tag{34}$$

$$T_0(k) = \frac{\left(\frac{c_d A_f \rho v(k)^2}{2} + m_{\text{veh}} g c_r \cos(\beta(k)) + m_{\text{veh}} g \sin(\beta(k)) + m_{\text{veh}} a(k)\right) rw}{i_0} + \frac{J_{\text{veh}} a(k)}{r_w i_0} \tag{35}$$

$$T_1(k) = \frac{m_{\text{bat,base}} (g c_r \cos(\beta(k)) + g \sin(\beta(k)) + a(k)) rw}{i_0} \tag{36}$$

$$T_2(k) = \frac{m_{\text{EM1,base}} (g c_r \cos(\beta(k)) + g \sin(\beta(k)) + a(k)) rw}{i_0} \tag{37}$$

$$T_3(k) = \frac{m_{\text{EM2,base}} (g c_r \cos(\beta(k)) + g \sin(\beta(k)) + a(k)) rw}{i_0}. \tag{38}$$

TABLE V
PERFORMANCE OF THE BUS DRIVING CYCLE

Performance	value	unit
max speed	68.83	km/h
Distance	16.55	km
Max acceleration	0.84	m/s^2
Average speed	19.60	km/h

One of the advantages of an electric bus is that its driving route is typically fixed. Here we adopted a real city driving cycle (Gothenburg, Sweden), which is shown in Fig. 5. The performance of driving cycle is listed in Table V. According to the performance and vehicle parameters, the main design criteria of the powertrain system are fulfilled optimally via convex programming.

Given the relevant equations listed in Section II and the foregoing objective function, the optimization problem is formulated in Table VI.

As mentioned before, the clutch control torque T^* is optimized through an outer-loop algorithm. The associated pseudocode is given below:

$$\begin{aligned}
&\text{temp}\,T^* = 1:1:\max(T_{\text{dem}})\\
&\text{for}\,j = 1:1:\text{numel}(\text{temp}T^*)\\
&\quad \text{tempcost}(j) = \min\text{cost}\\
&\text{end}\\
&\text{for}\,i = 1:1:\text{numel}(\text{tempcost})\\
&\quad \text{if tempcost}(i) = \min\ \text{tempcost}\\
&\qquad T^* = \text{temp}\,T^*(i)\\
&\quad \text{end}\\
&\text{end}.
\end{aligned}$$

IV. RESULTS AND DISCUSSION

In this section, we illustrate optimization results and demonstrate the effectiveness and time efficiency of the combined power-source sizing and control approach.

A. Comparative Analysis of Four Optimization Scenarios

First, we consider four different scenarios below for a comprehensive comparison (each scenario is able to satisfy the driving performance of the bus, i.e., tracking the driving cycle well)

1) s_{EM1} and s_{EM2} are kept to 1 during the optimization with the clutch operation;
2) s_{EM1} and s_{EM2} are optimized with the clutch operation;
3) s_{EM1} and s_{EM2} are kept to 1 during the optimization without the clutch;
4) s_{EM1} and s_{EM2} are optimized without the clutch.

The associated outcomes of the four cases under the Gothenburg driving cycle are reported in Table VII.

When assuming no clutch in the powertrain, in the case 4), the total cost is 28.50 euro/100 km, saving approximately 5.36%, compared to the case 3) with pre-fixed motor sizes. The optimization result of the case 4) indicates that the EM1 size is zero,

TABLE VI
OPTIMIZATION FRAMEWORK

Objective function: min cost

Optimization variables: $E_{\text{bat}}(N+1), T_{\text{EM}i}(N), s_{\text{bat}}, s_{\text{EM}i}$ (N is the number of time steps in a given drive cycle and i =1, 2.)

Expressions: $\tilde{P}_{\text{bat,total}}(N), V_{\text{oc}}{}^2(N), \tilde{P}_{\text{bat,loss}}(N), P_{\text{EM}i,\text{loss}}(N), P_{\text{EM}i}(N)$

$$\tilde{P}_{\text{bat,total}} = (E_{\text{bat}}(1:N) - E_{\text{bat}}(2:N+1))/\Delta t$$

$$V_{\text{oc}}{}^2 = \frac{2E_{\text{bat}}(1:N)}{n_{\text{bat,base}} s_{\text{bat}} C} + V_0{}^2$$

$$\tilde{P}_{\text{bat,loss}} = \frac{\tilde{P}^2_{\text{bat,total}}}{V_{\text{oc}}{}^2 n_{\text{bat,base}} s_{\text{bat}}} R$$

$$P_{\text{EM}i} = P_{\text{EM}i,\text{input}} - P_{\text{EM}i,\text{loss}}$$

$P_{\text{EM}i,\text{loss}}(k)$ and $P_{\text{EM}i,\text{input}}(k)$ are formulated by (13) and (14).

Constraints:

When the vehicle is in steady state:

$$P_{\text{dem}}(k) = 0$$
$$\tilde{P}_{\text{bat,total}}(k) \geq \tilde{P}_{\text{bat,loss}}(k) + P_{\text{aux}}$$

While the vehicle is moving:

If the necessary condition is satisfied for the clutch engagement:

$$e_{\text{clutch}} = 1$$
$$T_{\text{EM1}}(k) + T_{\text{EM2}}(k) \geq T_0(k) + T_1(k) s_{\text{bat}} + T_2(k) s_{\text{EM1}} + T_3(k) s_{\text{EM2}}$$
$$\tilde{P}_{\text{bat,total}}(k) \geq \tilde{P}_{\text{bat,loss}}(k) + P_{\text{aux}} + P_{\text{EM1,input}}(k) + P_{\text{EM2,input}}(k)$$

If the necessary condition is not satisfied:

$$e_{\text{clutch}} = 0$$
$$T_{\text{EM2}}(k) = 0$$
$$T_{\text{EM1}}(k) \geq T_0(k) + T_1(k) s_{\text{bat}} + T_2(k) s_{\text{EM1}} + T_3(k) s_{\text{EM2}}$$
$$\tilde{P}_{\text{bat,total}}(k) \geq \tilde{P}_{\text{bat,loss}}(k) + P_{\text{aux}} + P_{\text{EM1,input}}(k)$$

In order to improve numerical properties of optimization, we set an additional motor size constraint:

$$s_{\text{EM1}} + s_{\text{EM2}} \leq 2$$

this setting can meet the peak power demand of 138.27 kW in, e.g., the drive cycle in Fig. 5.

The remaining constraints include (24), (25), and

$$T_{\text{EM}i}(k) \in [T_{\text{EM}i\min,\text{base}},\ T_{\text{EM}i\max,\text{base}}] s_{\text{EM}i}$$
$$P_{\text{EM}i} \in [P_{\text{EM}i\min,\text{base}}, P_{\text{EM}i\max,\text{base}}] s_{\text{EM}i}$$
$$E_{\text{bat}} \in \frac{C}{2}[V_{\text{oc}}{}^2(SOC_{\min}), V_{\text{oc}}{}^2(SOC_{\max})] n_{\text{bat,base}} s_{\text{bat}}$$
$$s_{\text{bat}} \in [s_{\text{bat,min}}, s_{\text{bat,max}}]$$
$$s_{\text{EM}i} \in [s_{\text{EM}i,\min}, s_{\text{EM}i,\max}]$$

TABLE VII
RESULTS OF FOUR DIFFERENT SCENARIOS

The torque split is optimized.	Total Cost [euro/100 km]	Battery [kWh]	EM1 [kW]	EM2 [kW]	T^* [Nm]
1)	28.37	30.87	70	100	530
2)	27.91	30.60	28.95	110.47	246
3)	30.11	32.84	70	100	/
4)	28.50	31.36	0	139.48	/

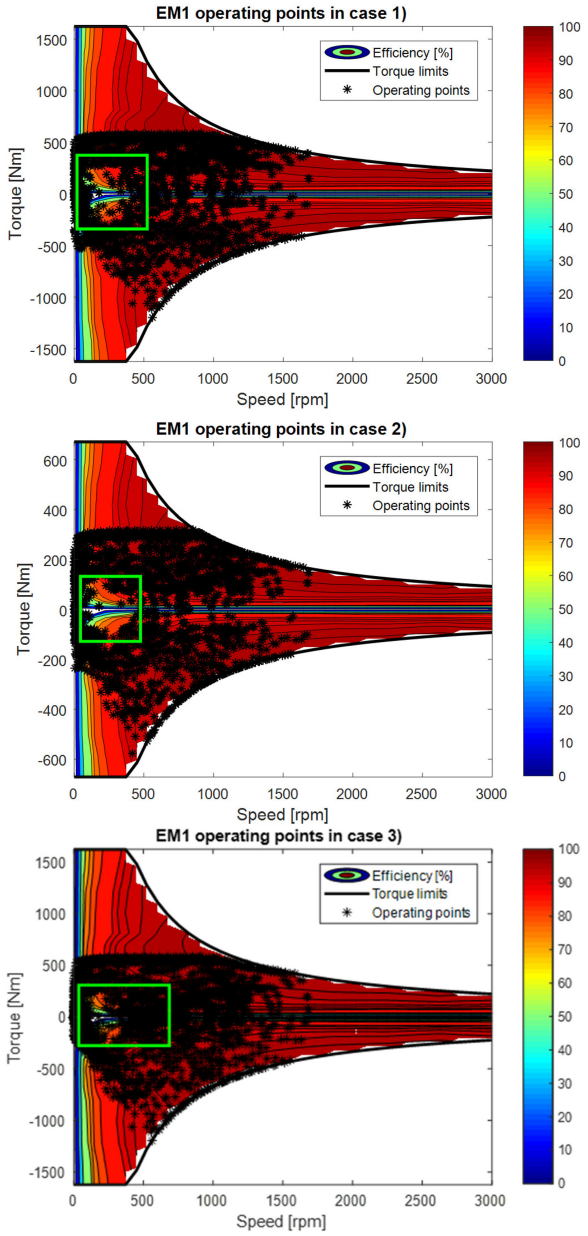

Fig. 6. EM1 operating points in the cases 1)–3). The green rectangle highlights low-efficiency region.

and the EM2 size is 139.48 kW. This observation implies that an appropriately sized motor, together with a well-sized battery pack, is more economical than a dual-motor counterpart, in the case of no clutch.

It is thus interesting to further examine whether the utilization of the clutch reduces the total cost and affects the battery and motor sizes. The result of the case 2) shows that the total cost is 27.91 euro/100 km, further saving 2.05% versus the case 4). The optimized sizes of EM1 and EM2 are 28.95 kW and 110.47 kW, respectively. It reveals that the clutch operation only has a significant impact on the EM1 size (i.e., a noticeable contribution to reduction of the EM1 size versus the baseline one). The reason is that EM2 is turned OFF when the torque demand is less than the optimal clutch control torque T^* of 246 Nm, and then a small EM1 is merely needed to propel the vehicle at very low load.

The operating points superimposed on efficiency maps of EM1 in the cases 1)–3) are plotted in Fig. 6. It can be observed that EM 1 in the cases 1) and 3) more frequently operate in low-efficiency region (the green solid rectangle), leading to more power losses, compared to the case 2). The operating points and efficiency of EM2 in the four cases are shown in Fig. 7. On the one hand, in contrast to the cases 1) and 3), the operating points of EM2 in the optimal case 2) are obviously more in high-efficiency region (the green dash rectangle). On the other hand, the EM2 operating points in low-efficiency region (the green solid rectangle) in the case 2) are significantly less than those in the cases 3) and 4). All of these contribute to reduced EM2 power losses and thus higher overall energy conversion efficiency.

The torque split outcome between the two motors is shown in Fig. 8(a). Obviously, without the clutch, the EM1 and EM2 have almost the same torque in the case 3), resulting in poor adaptability to varying torque demands for energy conservation. In the case 4), only the EM2 operates such that a large number of operating points locate in low-torque region with relatively low efficiency. Instead, the clutch in the cases 1) and 2) is clearly conducive to making the torque split more energy-efficient. Specifically, the EM2 will be isolated by the clutch at some low torque demands such that only the smaller EM1 works to seek increased efficiency. Moreover, compared to the case 1), the optimal solution [the case 2)] yields a significantly reduced EM1 and thereby a lower threshold for engaging the clutch. As such, the EM1-only mode in the case 2) induces higher energy efficiency when torque demands do not exceed 246 Nm.

The battery SOC trajectories of the four cases are shown in Fig. 8(b). It can be seen that the optimization of the battery size and the torque split between the two motors engenders similar SOC traces. Further, the optimal battery size of 30.60 kWh in the case 2) results in a downsized, economical energy storage integration. The associated size reductions are approximately 0.87%, 6.81%, and 2.42%, relative to the cases 1), 3), and 4), respectively. The clutch operation and the optimized EM1/EM2 sizes that increase the overall electric-drive energy conversion efficiency enable the battery downsizing. As opposed to passenger cars, for an electric bus, its battery can be often charged or swapped at the terminal station, i.e., the end of each driving

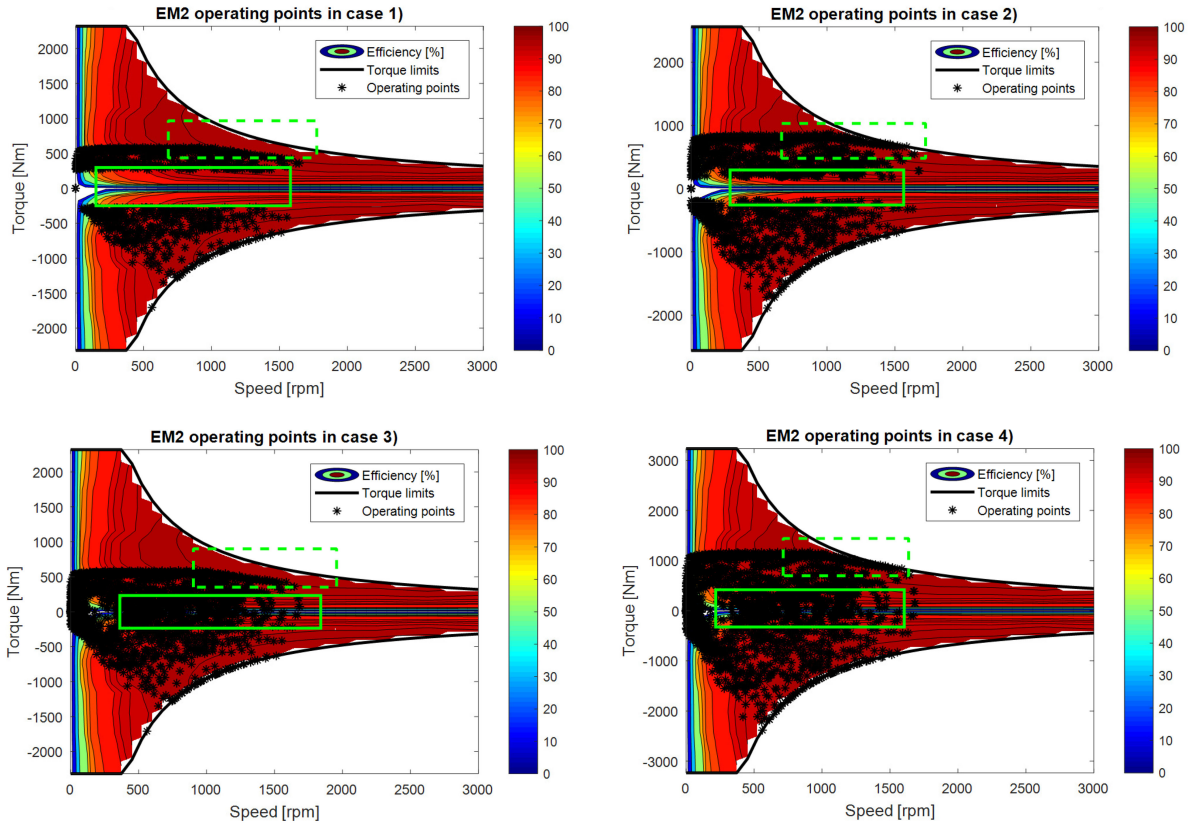

Fig. 7. EM2 operating points in the cases 1)–4). The green solid and dashed rectangles highlight low and high efficiency regions, respectively.

cycle. The optimized result can circumvent the overdesign of the battery system. An optimal battery size not only can cut the vehicle mass down, but also improve the vehicle dynamic performance. Of course, if we use longer driving cycles, the proposed convex programming method will yield bigger battery sizes, in order to seek the maximal vehicle economy while meeting the driving performance requirement of the adopted cycles.

B. Comparison of Different EM1/EM2 Sizes

To further verify the efficacy of the proposed sizing/control scheme, we perform an additional comparative study of options accounting for different EM1 and EM2 sizes. According to the optimal solution [see the case 2) in Table VII], the sum of the EM1 and EM2 power ratings equals to approximately 140 kW. To respect this total electric power constraint, four more scenarios with heuristic EM1/EM2 sizes are considered, where two common choices use identical EM1 and EM2 with/without the clutch, whereas the others employ discrepantly sized EM1/EM2 with the clutch. Note that these EM1/EM2 size in the four scenarios are fixed in the convex optimization that only optimize the battery size and the torque split. The corresponding results are displayed in Table VIII. It is evident that the common options using identical EM1 and EM2 are most costly, where the optimized EM1/EM2 torques give rise to an even torque distribution when both motors work, as analytically verified in [11]. In contrast, a combination of a smaller EM1 and a larger EM2 has the potential for reducing the total cost. In particular, the cost of the optimal case 2) is about 1.31% lower than that of using identical EM1/EM2 with the clutch. If the clutch is absent, the cost-saving advantage will increase to 5.42%.

C. Results Under Different Drive Cycles

The results discussed above correspond to the drive cycle of a city bus route in Gothenburg, Sweden (see Fig. 5). It is well known that driving patterns have a great influence on the performance, design, and control of vehicular powertrains. Therefore, it is beneficial to investigating the applicability of the proposed method under different drive cycles, as well as how varying driving patterns impact the sizing/control optimization outcome. To this end, in this section, two additional example drive cycles are taken into account, including Federal Test Procedure (FTP_HIGHWAY) from ADVISOR [55] for emulating highway driving and city suburban cycle (CSC) [56] for mixed urban and suburban driving, in order to capture driving characteristics in different bus applications, like a coach or a transit bus. Accordingly, before running the convex optimization routine, we need to re-set the constraint of the peak power demand, i.e., the sum of EM1/EM2 scaling factors. The associated updated constraints, as well as main characteristics of FTP_HIGHWAY and CSC are presented in Table IX. The optimization results are presented in Table X. The optimized EM1/EM2 sizes in FTP_HIGHWAY are 87 kW and 150.1 kW, which are higher than those in CSC (i.e., 42.5 kW and 109.2 kW), owing to higher peak power demands in the highway driving. In addition, versus CSC, the longer driving distance of FTP_HIGHWAY entails an

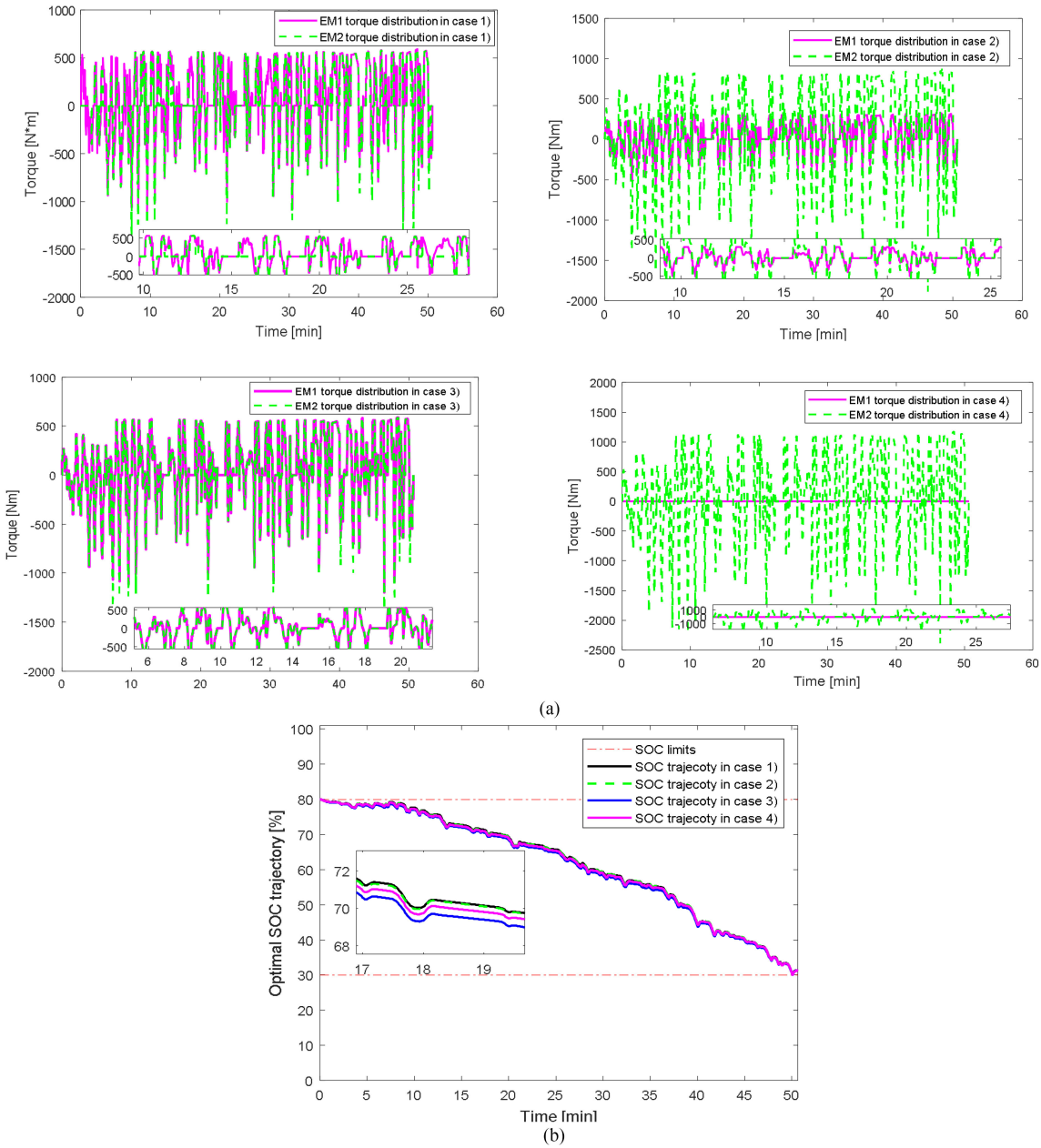

Fig. 8. (a) Torque split outcome in the four cases. (b) Optimal SOC trajectories.

TABLE VIII
RESULTS OF DIFFERENT EM1/EM2 SIZES

The torque split is optimized.	Total Cost [euro/100 km]	Battery [kWh]	EM1 [kW]	EM2 [kW]	T^* [Nm]
	29.51	32.38	70	70	[-]
	28.28	31.01	70	70	530
	28.08	30.79	52.5	87.5	378
	28.05	30.75	35	105	248
Table VII, case 2)	27.91	30.60	28.95	110.47	246

TABLE IX
MAIN CHARACTERISTICS AND PEAK POWER CONSTRAINTS IN TWO EXAMPLE CYCLES

Drive cycle	Time [s]	Distance [km]	Max. Speed [km/h]	Ave. Speed [km/h]	Max. P_{dem} [kW]	Constraint
FTP_HIGHWAY	765	16.49	96.3	77.62	233.47	$s_{EM1} + s_{EM2} <= 3.5$
CSC	1701	10.75	70.55	22.75	151.48	$s_{EM1} + s_{EM2} <= 2.5$

TABLE X
RESULTS IN TWO ADDITIONAL CYCLES

Drive cycle	Total Cost [euro/100 km]	Battery [kWh]	EM1 [kW]	EM2 [kW]	T^* [Nm]
FTP_HIGHWAY	30.02	32.58	87.00	150.1	372
CSC	23.26	18.49	42.50	109.2	374

TABLE XI
COMPUTATIONAL TIME

Driving cycle	Gothenburg	FTP_HIGHWAY	CSC
Time [s][1]	21.84	1.92	5.73

[1]A 2.5 GHz microprocessor with 4 GB RAM was used.

enlarged battery pack to provide enough energy. Consequently, the total cost of 30.02 euro/100km in FTP_HIGHWAY is approximately 29.06% higher than that in CSC. Again, it should be emphasized that the optimal EM1/EM2 sizes are not equal in both cycles, with uneven torque distribution between both motors, which is not plotted here for simplicity.

D. Computational Efficiency

Indeed, integration of multiple power sources into electrified powertrains is usually a difficult and laborious task, due to a clear multiplicity of power-source technology choice, topology, sizing, and control. As a result, computational efficiency of algorithms is still heavily concerned in developing vehicular propulsion systems, even for some offline designs, with the pursuit of cutting time and cost down. It is therefore important to examine the computational efficiency of the optimization method used in this study. As presented in Table XI, given the pre-determined torque threshold T^* governing the clutch, the optimization is able to solve the power-source sizing and control problem within only 22 s, 2 s, and 6 s under the Gothenburg, FTP_HIGHWAY, and CSC cycles, respectively. This signifies that the algorithmic efficiency is very high, with a linear proportion to the distance of drive cycle.

V. CONCLUSION

This paper develops a convex programming based approach, innovatively enabling a quick, effective co-optimization of energy management strategy, battery dimension, and motor dimension for a dual-motor-driven electric bus powertrain. Numerous comparative results confirm that this approach can maximize the vehicle economy by optimizing electric-drive efficiency, through appropriately trading off the battery size, sizes of two motors, and power-flow control. The idea could furnish some inspiring insights into powertrain design optimization of multiple-motor-driven EVs. Several key observations are summarized as follows.

1) The optimized sizes of EM1 and EM2 in the Gothenburg drive cycle are 28.95 kW and 110.47 kW, respectively, rather than two equally sized motors. It can save the total cost by 1.31% and 5.42%, in comparison with those of using identical EM1/EM2 with/without the clutch. The optimal torque split between the optimized EM1 and EM2 is uneven, which makes both motors work in high-efficiency regions more frequently.
2) The increased EM1/EM2 efficiency is expedient to the battery pack downsizing.
3) The optimization routine is extensible to different drive cycles and thus help evaluate the implication of altered driving patterns.
4) The optimization routine solves the power-source sizing and control problem within 22 s, 2 s, and 6 s under the Gothenburg, FTP_HIGHWAY, and CSC cycles, respectively, highlighting a remarkable computational advantage.

REFERENCES

[1] W. Su, H. Rahimi-Eichi, W. Zeng, and M.-Y. Chow, "A survey on the electrification of transportation in a smart grid environment," *IEEE Trans. Ind. Inform.*, vol. 8, no. 1, pp. 1–10, Feb. 2012.
[2] C. D. Rahn and C. Y. Wang, *Battery Systems Engineering*. West Sussex, U.K.: Wiley, 2013.
[3] X. Hu, C. Zou, C. Zhang, and Y. Li, "Technological developments in batteries: A survey of principal roles, types, and management needs," *IEEE Power Energy Mag.*, vol. 15, no. 5, pp. 20–31, Sep. 2017.
[4] V. Etacheri, R. Marom, R. Elazari, G. Salitra, and D. Aurbach, "Challenges in the development of advanced Li-ion batteries: A review," *Energy Environ. Sci.*, vol. 4, no. 9, pp. 3243–3262, Jul. 2011.
[5] S. Chopra and P. Bauer, "Driving range extension of EV with on-road contactless power transfer—A case study," *IEEE Trans. Ind. Electron.*, vol. 60, no. 1, pp. 329–338, Jan. 2013.
[6] H. Liu, X. Chen, and X. Wang, "Overview and prospects on distributed drive electric vehicles and its energy saving strategy," *Prz. Elektrotech.(Elect. Rev.)*, vol. 88, no. 7a, pp. 122–125, 2012.
[7] N. Mutoh, T. Kazama, and K. Takita, "Driving characteristics of an electric vehicle system with independently driven front and rear wheels," *IEEE Trans. Ind. Electron.*, vol. 53, no. 3, pp. 803–813, Jun. 2006.
[8] B. Lu, H. Chen, H. He, and J. Peng, "The dynamic matching calculation and simulation for dual-motor driven electric vehicle." in *Proc. IEEE Transp. Electrific. Asia-Pacific (ITEC Asia-Pacific) Conf. Expo.*, Beijing, China, 2014, pp. 1–5.
[9] C.-H. Yu, C.-Y. Tseng, and C.-M. Chang, "Study on power train of two axles four wheel drive electric vehicle," *Energy Procedia*, vol. 14, pp. 1528–1535, 2012.
[10] B. Sun, S. Gao, C. Ma, and J. Li, "System power loss optimization of electric vehicle driven by front and rear induction motors," *Int. J. Automot. Technol.*, vol. 19, no. 1, pp. 121–134, Feb. 2018.
[11] X. Yuan and J. Wang, "Torque distribution strategy for a front-and rear-wheel-driven electric vehicle," *IEEE Trans. Veh. Technol.*, vol. 61, no. 8, pp. 3365–3374, Oct. 2012.
[12] Z. Yang, J. Wang, G. Gao, and X. Shi, "Research on optimized torque-distribution control method for front/rear axle electric wheel loader," *Math. Problems Eng.*, vol. 2017, 2017, doi:10.1155/2017/7076583, Art. no. 7076583.
[13] D. Wang and B. Wang, "Research on driving force optimal distribution and fuzzy decision control system for a dual-motor electric vehicle." in *Proc. 34th Chin. Control Conf.,* Hangzhou, China, 2015, pp. 8146–8153.
[14] (Jan. 2018). [Online]. Available: https://www.tesla.com/models
[15] P. D. U. Coronado and H. Ahuett-Garza, "Control strategy for power distribution in dual motor propulsion system for electric vehicles," *Math. Problems Eng.*, vol. 2015, 2015. doi:10.1155/2015/814307, Art. no. 814307.
[16] M. Hu, J. Zeng, S. Xu, C. Fu, and D. Qin, "Efficiency study of a dual-motor coupling EV powertrain," *IEEE Trans. Veh. Technol.*, vol. 64, no. 6, pp. 2252–2260, Jun. 2015.
[17] S. Zhang, C. Zhang, G. Han, and Q. Wang, "Optimal control strategy design based on dynamic programming for a dual-motor coupling-propulsion system," *Sci. World J.*, vol. 2014, 2014. doi:10.1155/2014/958239, Art. no. 958239.
[18] C. Li, Y. Li, W. Xiao, J. Hu, and L. Zhao, "Parameters optimization of dual-motor EV powertrain for energy consumption," (in Chinese), *Comput. Integr. Manuf. Syst.*, vol. 23, no. 8, pp. 1620–1628, Aug. 2016.

[19] Y. Wang and D. Sun, "Powertrain matching and optimization of dual-motor hybrid driving system for electric vehicle based on quantum genetic intelligent algorithm," *Discrete Dyn. Nature Soc.*, vol. 2014, 2014, doi:10.1155/2014/956521, Art. no. 956521.
[20] C. Zhang, S. Zhang, G. Han, and H. Liu, "Power management comparison for a dual-motor-propulsion system used in a battery electric bus," *IEEE Trans. Ind. Electron.*, vol. 64, no. 5, pp. 3873–3882, May 2017.
[21] Y. Tang, "Dual motor drive and control system for an electric vehicle," U.S. Patent 20100222953A1, May 18, 2010.
[22] A. D. Keyser, M. Vandeputte, and G. Crevecoeur, "Convex mapping formulations enabling optimal power split and design of the electric drivetrain in all-electric vehicles," *IEEE Trans. Veh. Technol.*, vol. 66, no. 11, pp. 9702–9711, Nov. 2017.
[23] J. Zhu *et al.*, "Dual-motor power system and dual-motor hybrid power system for vehicle," U.S. Patent 9789754B2, Oct. 17, 2017.
[24] D. Cesiel, M. C. Gaunt, and B. Daugherty, "Development of a steer-by-wire system for the GM Sequel," presented at *SAE 2006 World Congr. Exhib.*, Detroit, MI, USA, SAE Paper 2006-01-1173, 2006.
[25] M. Sundar and D. Plunkett, "Brake-by-wire, motivation and engineering—GM Sequel," presented at *24th Annu. Brake Colloq. Exhib.*, Grapevine, TX, USA, SAE Paper 2006-01-3194, 2016.
[26] Y. Chen, X. Li, C. Wiet, and J. Wang, "Energy management and driving strategy for in-wheel motor electric ground vehicles with terrain profile preview," *IEEE Trans. Ind. Inform.*, vol. 10, no. 3, pp. 1938–1947, Aug. 2014.
[27] A. M. Dizqah, B. Lenzo, A. Sorniotti, P. Gruber, S. Fallah, and J. de Smet, "A fast and parametric torque distribution strategy for four-wheel-drive energy-efficient electric vehicles," *IEEE Trans. Ind. Electron.*, vol. 63, no. 7, pp. 4367–4376, Jul. 2016.
[28] B. Lenzo *et al.*, "Torque distribution strategies for energy-efficient electric vehicles with multiple drivetrains," *J. Dyn. Syst. Meas. Control*, vol. 139, no. 12, Dec. 2017, Art. no. 121004.
[29] D. Wu, Y. Li, J. Zhang, and C. Du, "Torque distribution of a four in-wheel motors electric vehicle based on a PMSM system model," in *Proc. IMechE. Part D: J. Automobile Eng.*, 2017, pp. 1–18.
[30] H. Qian, G. Xu, J. Yan, T. Lam, Y. Xu, and K. Xu, "Energy management for four-wheel independent driving vehicle." in *Proc. IEEE/RSJ Int. Conf. Intell. Robots Syst.*, Taipei, Taiwan, 2010, pp. 5532–5537.
[31] C. Lin and Z. Xu, "Wheel torque distribution of four-wheel-drive electric vehicles based on multi-objective optimization," *Energies*, vol. 8, no. 5, pp. 3815–3831, 2015.
[32] Z. Wang, C. Qu, X. Xue, and L. Zhang, "Design and control strategy optimization for four-wheel independently actuated electric vehicles," *Energy Procedia*, vol. 105, pp. 2323–2328, 2017.
[33] V. Ivanov, D. Savitski, and B. Shyrokau, "A survey of traction control and antilock braking systems of full electric vehicles with individually controlled electric motors," *IEEE Trans. Veh. Technol.*, vol. 64, no. 9, pp. 3878–3896, Sep. 2015.
[34] P. D. U. Coronado, P. O. Castañón, and H. Ahuett-Garza, "Optimization of gear ratio and power distribution for a multimotor powertrain of an electric vehicle," *Eng. Optim.*, vol. 50, no. 2, pp. 293–309, 2018.
[35] N. Murgovski, L. Johannesson, J. Sjöberg, and B. Egardt, "Component sizing of a plug-in hybrid electric powertrain via convex optimization," *Mechatronics*, vol. 22, no. 1, pp. 106–120, Feb. 2012.
[36] B. Egardt, N. Murgovski, M. Pourabdollah, and L. Johannesson, "Electromobility studies based on convex optimization: Design and control issues regarding vehicle electrification," *IEEE Control Syst. Mag.*, vol. 34, no. 2, pp. 32–49, Apr. 2014.
[37] M. Pourabdollah, N. Murgovski, A. Grauers, and B. Egardt, "Optimal sizing of a parallel PHEV powertrain," *IEEE Trans. Veh. Technol.*, vol. 62, no. 6, pp. 2469–2480, Jul. 2013.
[38] X. Hu, S. J. Moura, N. Murgovski, B. Egardt, and D. Cao, "Integrated optimization of battery sizing, charging, and power management in plug-in hybrid electric vehicles," *IEEE Trans. Control Syst. Technol.*, vol. 24, no. 3, pp. 1036–1043, May 2016.
[39] X. Hu, L. Johannesson, N. Murgovski, and B. Egardt, "Longevity-conscious dimensioning and power management of the hybrid energy storage system in a fuel cell hybrid electric bus," *Appl. Energy*, vol. 137, pp. 913–924, Jan. 2015.
[40] M. Pourabdollah, B. Egardt, N. Murgovski, and A. Grauers, "Convex optimization methods for powertrain sizing of electrified vehicles by using different levels of modeling details," *IEEE Trans. Veh. Technol.*, vol. 67, no. 3, pp. 1881–1893, Mar. 2018.
[41] C. S. N. Shiau, N. Kaushal, C. T. Hendrickson, S. B. Peterson, J. F. Whitacre, and J. J. Michalek, "Optimal plug-in hybrid electric vehicle design and allocation for minimum life cycle cost, petroleum consumption, and greenhouse gas emissions," *J. Mech. Design*, vol. 132, no. 9, pp. 091013-1–091013-11, Sep. 2010.
[42] O. Sundström, "Optimal control and design of hybrid electric vehicles," Ph.D. dissertation, ETH Univ., Zurich, Switzerland, 2009.
[43] X. Wu, B. Cao, X. Li, J. Xu, and X. Ren, "Component sizing optimization of plug-in hybrid electric vehicles," *Appl. Energy*, vol. 88.no. 3, pp. 799–804, Mar. 2011.
[44] S. E. Plotkin and M. K. Singh, "Multipath transportation futures study: Vehicle characterization and scenario analyses," *Argonne Nat. Lab.*, Lemont, IL, USA, Rep. ANL/ESD/09-5, 2009.
[45] X. Hu, N. Murgovski, L. M. Johannesson, and B. Egardt, "Comparison of three electrochemical energy buffers applied to a hybrid bus powertrain with simultaneous optimal sizing and energy management," *IEEE Trans. Intell. Transp. Syst.*, vol. 15, no. 3, pp. 1193–1205, Jun. 2014.
[46] (Jun. 2011). [Online]. Available: http://www.robotcombat.com/products/images/bp_configs/pdf/ANR26650M1.pdf
[47] N. Murgovski, L. Johannesson, A. Grauers, and J. Sjoberg, "Dimensioning and control of a thermally constrained double buffer plug-in HEV powertrain," in *Proc. IEEE 51st Annu. Conf. Decis. Control*, 2012, pp. 6346–6351.
[48] E. Walid, Y. Zhang, N. Natarajan, F. Massey, and C. C. Mi, "Model reference adaptive control for hybrid electric vehicle with dual clutch transmission configurations," *IEEE Trans. Veh. Technol.*, vol. 67, no. 2, pp. 991–999, Feb. 2018.
[49] Z. Zhao, X. Li, L. He, C. Wu, and J. K. Hedrick, "Estimation of torques transmitted by twin-clutch of dry dual-clutch transmission during vehicle's launching process," *IEEE Trans. Veh. Technol.*, vol. 66, no. 6, pp. 4727–4741, Jun. 2017.
[50] S. Kim, J. J. Oh, and S. B. Choi, "Driveline torque estimations for a ground vehicle with dual-clutch transmission," *IEEE Trans. Veh. Technol.*, vol. 67, no. 3, pp. 1977–1989, 2018.
[51] S. Boyd and L. Vandenberghe, *Convex Optimization*. Cambridge, U.K.: Cambridge University Press, 2004.
[52] M. Grant and S. Boyd, *CVX: Matlab Software for Disciplined Convex Programming, Version 2.0 Beta*.(2013). [Online]. Available: http://cvxr.com/cvx
[53] M. Pourabdollah, B Egardt, N Murgovski, and A. Grauers, "Effect of driving, charging, and pricing scenarios on optimal component sizing of a PHEV," *Control Eng. Pract.*, vol. 61, pp. 217–228, Apr. 2017.
[54] (Oct. 2017). [Online]. Available: http://ec.europa.eu/eurostat/statistics-explained/index.php/File:Electricity_prices,_second_half_of_year
[55] K. B. Wipke, M. R. Cuddy, and S. D. Burch, "ADVISOR 2.1: A user-friendly advanced powertrain simulation using a combined backward/forward approach," *IEEE Trans. Veh. Technol.*, vol. 48, no. 6, pp. 1751–1761, Nov. 1999.
[56] (Jan. 2018). [Online]. Available: https://www.dieselnet.com/standards/cycles/csc.php

Xiaosong Hu (SM'16) received the Ph.D. degree in automotive engineering from the Beijing Institute of Technology, China, in 2012.

He did scientific research and completed the Ph.D. dissertation at the Automotive Research Center, University of Michigan, Ann Arbor, USA, between 2010 and 2012. He was a Postdoctoral Researcher with the Department of Civil and Environmental Engineering, University of California, Berkeley, USA, between 2014 and 2015, as well as with the Swedish Hybrid Vehicle Center and the Department of Signals and Systems at Chalmers University of Technology, Gothenburg, Sweden, between 2012 and 2014. He was also a Visiting Postdoctoral Researcher with the Institute for Dynamic systems and Control at Swiss Federal Institute of Technology (ETH), Zurich, Switzerland, in 2014. He is currently a Professor with the State Key Laboratory of Mechanical Transmissions and with the Department of Automotive Engineering, Chongqing University, Chongqing, China. His research interests include modeling and control of alternative powertrains and energy storage systems.

Dr. Hu was the recipient of several prestigious awards/honors, including Emerging Sustainability Leaders Award in 2016, EU Marie Currie Fellowship in 2015, ASME DSCD Energy Systems Best Paper Award in 2015, and Beijing Best Ph.D. Dissertation Award in 2013.

Yapeng Li received the B.S. degree from the Henan University of Technology, Henan, China, in 2016. He is currently working toward the Ph.D. degree with the Department of Automotive Engineering at Chongqing University, Chongqing, China.

His research interests include hybrid and electric vehicle powertrain design and control.

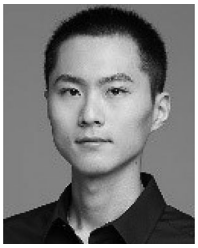

Chen Lv (S'14–M'16) received the Ph.D. degree from Tsinghua University, China, in 2016.

He was a Research Fellow with Advanced Vehicle Engineering Center, Cranfield University, U.K., during 2016 and 2018, and a Joint Ph.D. Researcher with EECS Department, University of California, Berkeley, USA, during 2014 and 2015. He is an Assistant Professor with the School of Mechanical and Aerospace Engineering, Nanyang Technological University, Singapore. His research interests include advanced vehicle control and intelligence, where he has contributed over 70 papers and obtained 12 granted China patents.

Dr. Lv serves as an Associate Editor for *Plos One*, *Automotive Innovation*, *International Journal of Electric and Hybrid Vehicles*, and *International Journal of Vehicle Systems Modelling and Testing*. He was the recipient of the Highly Commended Paper Award of IMechE UK in 2012, the China SAE Outstanding Paper Award in 2015, the Tsinghua University Outstanding Doctoral Thesis Award in 2016, and the Best Workshop/Special Session Paper Award of IEEE Intelligent Vehicle Symposium in 2018. He also serves as a Guest Editor for IEEE/ASME TRANSACTIONS ON MECHATRONICS, and IEEE TRANSACTIONS ON INDUSTRIAL INFORMATICS.

Yonggang Liu (M'18) was born in 1982. He received the Ph.D. degree from Chongqing University, Chongqing, China, in 2010.

He has worked as an Associate Professor and Doctoral Supervisor, and is currently a Dean Assistant with the School of Automotive Engineering, Chongqing University, Chongqing, China. He has led more than ten research projects, such as National Natural Science Foundation of China (both Youth Fund and General Program), Ph.D. Programs Foundation of Ministry of Education of China, and China Postdoctoral Science Foundation. The research projects which he has participated in, include Key Program of National Natural Science Foundation of China, National Key Research and Development Program of China during the 13th Five-Year Plan Period, Major State Basic Research Development Program of China (973 Program), National High Technology Research and Development Program of China (863 Program), and so on. He has authored more than 40 research papers and 9 of his patents have been awarded. His research interests include optimization and control of intelligent electric vehicles (EV/HEV) power system, and integrated control of vehicle automatic transmissions.

Dr. Liu served as the Head of the Secretariat for The International Conference on Power Transmissions (ICPT2016), the Session Chairman for the International Symposium on Electric Vehicles (ISEV2017), and the Committeeman of Technical Committee on Vehicle Control and Intelligence of Chinese Association of Automation (CAA). He was the recipient of the titles of "Advanced Worker of Chongqing University" and "The Most Popular Teacher of Chongqing University" for his work toward the teaching and scientific research of vehicle engineering. He is the Reviewer for the IEEE TRANSACTIONS ON VEHICULAR TECHNOLOGY, *Mechanism and Machine Theory*, *Applied Mathematical Modelling*, etc.